Available online at www.sciencedirect.com
SCIENCE DIRECT®
Biochemical Pharmacology 65 (2003) 1151–1161
Biochemical Pharmacology
www.elsevier.com/locate/biochempharm

Regulation of mastoparan-induced increase of paracellular permeability in T84 cells by RhoA and basolateral potassium channels

Irina Blumenstein[a,1], Ralf Gerhard[a,1], Jürgen Ries[a], Gabor Kottra[b], Jürgen Stein[a,*]

[a]*Division of Gastroenterology and Clinical Nutrition, 2nd Department of Medicine, Johann Wolfgang Goethe-Universität, Theodor-Stern-Kai 7, 60590 Frankfurt/Main D-60590, Germany*
[b]*Department of Physiology, Johann Wolfgang Goethe-Universität, Frankfurt/Main, Germany*

Received 13 August 2002; accepted 8 January 2003

Abstract

Mastoparan, a polypeptide known to activate heterotrimeric GTP-binding proteins, enhances the transport of Ca^{2+} and K^+ across membranes. In the present study we investigated the influence of mastoparan on transepithelial resistance (TER) and on short circuit current (SCC) of the intestinal cell line T84. Mastoparan decreased the TER by 80% of baseline and induced a SCC of 8.34 ± 1.38 μA cm^{-2}. The changes in paracellular conductance were estimated using the nystatin technique and showed that mastoparan increased the paracellular conductance 4-fold. Basolateral Cl^--free medium, or blockade of the basolateral Cl^- uptake *via* the $Na^+/K^+/2Cl^-$ co-transporter with bumetanide, reduced SCC of T84 cells, but did not abolish the effect of mastoparan on the TER. Luminal addition of the Cl^--channel blocker DIDS or NPPB had no effect on the increase in SCC. In contrast, blocking the basolateral K^+-channels by 2 mM Ba^{2+} inhibited both the resistance decrease and elevation of the SCC, and further inhibited the mastoparan-induced increase in intracellular free Ca^2. This indicates that mastoparan acts primarily *via* activating K^+ channels with a secondary Cl^- secretion and Ca^{2+} influx. Reduction of intracellular free Ca^{2+} did not alter the effect of mastoparan on TER. Stimulation with mastoparan led to a biphasic rearrangement of actin filaments and increased globular actin content in T84 cells. Depolymerization of actin filaments also correlated with inactivation of Rho-proteins, which are known regulators of the cytoskeleton. Mastoparan induced a 2-fold increase in GDI-complexed Rho.

We conclude that mastoparan-induced changes in paracellular permeability are mediated *via* enhanced basolateral K^+ conductance and Rho-protein inactivation. A secondary increase in intracellular Ca^{2+} or direct interaction of small GTPases with the cytoskeleton are likely mediators of the remodeling of the cytoskeleton with subsequent changes in paracellular permeability.

Keywords: Actin disassembling; Nystatin technique; Paracellular; Permeability; Potassium conductance; Short circuit current; Transepithelial resistance

1. Introduction

Intestinal tight junctions act as a barrier between the mucosal and serosal compartments of intestinal epithelia and thus limit the diffusion of molecules across epithelial cell monolayers. Hydrophilic and charged drugs, given perorally, are absorbed mostly *via* the paracellular route. Some drugs alter intestinal permeability in animals and humans [1]. Understanding the mechanisms of tight junction regulation is therefore of an utmost importance, both in physiology and pharmacology. Several lines of evidence suggest that tight junctions are dynamic rather than static structures, undergoing continuous assembling and disassembling. While it has been well-documented that a number of intracellular mediators (cAMP, cGMP, Ca^{2+}, and G-proteins) are involved, the intracellular regulation of intestinal tight junctions is still not completely defined.

Mastoparan (mas), an amphiphilic tetradecapeptide isolated from wasp venom with the structure Ile-Asn-Leu-Lys-Ala-Leu-Ala-Lys-Lys-Ile-Leu-NH_2, has been reported by several authors to specifically activate G-proteins and

* Corresponding author. Tel.: +49-69-6301-5917; fax: +49-69-6301-83112.
E-mail address: j.stein@em.uni-frankfurt.de (J. Stein).
[1] I.B. and R.G. contributed equally to this manuscript.
Abbreviations: GTP, guanosine 5′-triphosphate; DIDS, 4,4′-diisothiocyanatostilbene-2,2′-disulfonic acid; NPPB, 5-nitro-2-(3-phenylpropylamino)benzoic acid; GDI, guanine nucleotide dissociation inhibitor; NSAID, nonsteroidal antiinflammatory drug; cAMP, adenosine 3′,5′-cyclicmonophosphate; cGMP, guanosine 3′,5′-cyclicmonophosphate; mas, mastoparan; NCS, new-born calf serum; VIP, vasointestinal peptide; TER, transepithelial resistance; SCC, I_{sc}, short circuit current; EGTA, ethylene glycol-bis(2-aminoethylether)-*N*,*N*,*N*′,*N*′-tetraacetic acid; $[Ca^{2+}]_i$, intracellular calcium; BAPTA, ethylenedioxybis-(*o*-phenylenenitrilo)tetraacetic acid.

0006-2952/03/$ – see front matter © 2003 Elsevier Science Inc. All rights reserved.
doi:10.1016/S0006-2952(03)00043-1

G-protein coupled potassium channels [2–9]. Winter *et al*. first demonstrated alterations of paracellular permeability resulting from direct activation of potassium and chloride conductance by mastoparan in the renal epithelial cell line MDCK [10]. Mastoparan also increases intracellular Ca^{2+} in several cell lines [11,12] and the intracellular cAMP level [13]. A new evidence suggests that small G-proteins are involved in the control of tight junction permeability [14]. Koch *et al*. showed the interaction of mastoparan with low mass GTP-binding proteins of the rho/rac family in porcine brain [15]. Further observations indicated important links between tight junctions and cytoskeletal elements, especially actin filaments [16,17].

The objective of this study was to define whether mastoparan influences paracellular permeability in the human colon carcinoma cell line T84 and, if so, to elucidate intracellular signal transduction pathways involved.

2. Materials and methods

2.1. Materials

T84 cells were a generous gift of Prof. K.E. Barrett, University of California. Cell culture media were obtained from Pan systems (Aidenbach) and NCS from Serva. All other cell culture supplements were from Gibco. Permeable supports for Snapwell™ diffusion chambers were obtained from Costar. Fura-2 AM and rhodamine-phalloidin were purchased from Molecular Probes. Mastoparan (mas) was obtained from Bachem, mas7, mas17, NPPB, and bumetanide from Biomol (Plymouth Meeting). Glibenclamide, 4,4′-diisothiocyanato-stilbene-2,2′-disulfonic acid (DIDS), nystatin, vasoactive intestinal peptide (VIP), forskolin, bovine muscle actin, deoxyribonucleic acid I from calf thymus and deoxyribonuclease I, type IV, were purchased from Sigma. *N*-Phenylanthranilic acid was obtained from Merck, and myo-[1,2-^{3}H(*N*)]-inositol, D-[2^{3}H(*N*)]-inositol-1-phosphate, D-[2^{3}H(*N*)]-inositol-1,4-bisphosphate, D-[1^{3}H(*N*)]-inositol-1,3,4-trisphosphate, D-[1^{3}H(*N*)]-inositol-1,4,5-trisphosphate, D-[1^{3}H(*N*)]-inositol-1,3,4,5-tetrakisphosphate, [2^{3}H(*N*)]-myoinositolhexakis-phosphate and ^{125}iodine from NEN du Pont. All chemicals were of the purest quality available.

2.2. Methods

2.2.1. Cell culture

T84 cells (passages 20–44) were grown in DMEM/F12 mix (1:1), supplemented with 5% NCS, 100 U mL^{-1} penicillin and 100 μg mL^{-1} streptomycin. The medium was changed every other day. Cells were subcultured every 14 days (Dulbecco's PBS containing 0.25% trypsin, 0.1% EDTA). For electrophysiological measurement the cells were seeded at a density of 5×10^5 cm^{-2} on permeable supports (Snapwell™, 1 cm^2 surface area) and grown until total confluency.

To determine whether the effects of mastoparan influenced cytolysis or cell detachment, T84 cells were seeded on coverslips and cultured until confluent. The cells were incubated in bicarbonate-buffered Ringer solution with 19 mM glucose with or without 10 μM mastoparan for 45 min. After incubation cells were washed three times with PBS and the incorporated ethidium homodimer as a marker of cell death was detected spectrophotometrically (em = 590 nm).

2.3. Measurement of electrical parametres

The permeable supports bearing confluent monolayers were mounted on Snapwell™ diffusion chambers 7–10 days after plating. Only T84 monolayer with initial resistances $\geq$1000 Ω cm^2 were used for experiments. Each experiment was initiated after a 30 min equilibration period with a stable baseline resistance present. Bicarbonate buffered Ringer solution (115 mM NaCl, 1.2 mM $MgCl_2$, 1.2 mM $CaCl_2$, 2.4 mM K_2HPO_4, 0.4 mM KH_2PO_4, 25 mM $NaHCO_3$) supplemented with 10 mM glucose was used in apical and basolateral chambers and was circulated by bubbling with 5% CO_2 in air. In some experiments the basolateral but not the apical Ringer solution was substituted with chloride-free Ringer (115 mM isethionate, sodium salt, 1.2 mM $MgSO_4$, 1.2 mM $CaSO_4$, 2.4 mM K_2HPO_4, 0.4 mM KH_2PO_4, 25 mM $NaHCO_3$, 10 mM glucose). Open circuit transepithelial potential differences (V_t) were measured by calomel electrodes immersed in saturated KCl, connected with agarose bridges (4% agarose in 0.9% NaCl solution) to the apical and basolateral reservoir. To calculate TER pulses of 10 μA cm^{-2}, 0.9 s duration were generated every 150 s (MCC6, Physiologic Instruments) and TER was calculated from the resulting transepithelial voltage deflections and the density of applied current. Because of variation of initial resistances of the monolayer, the data on TERs are presented as a percentage of the mean baseline resistance. SCC was calculated from V_t and TER.

Paracellular conductance and the apical membrane conductance of T84 cells were measured using the nystatin technique, first described by Wills *et al*. (1979). The resistance of the apical membrane was progressively reduced by addition of 400 U mL^{-1} nystatin to the apical reservoir. Transepithelial conductance was plotted as function of SCC and, paracellular conductance was calculated as the intercept of the fitted linear function with the conductance axis.

2.4. Isotopic flux studies

The *paracellular* transport was measured by a modification of the method of Amelsberg *et al*. [18]. To determine paracellular flux, the cells were seeded at a density of 4×10^5 cells cm^{-2} on Millipore filter inserts (0.45 μM

pore size). To verify confluency of the monolayers, 0.5 μCi [^{14}C]mannitol together with unlabelled mannitol was added to the apical chamber as an inert flux marker (final concentration 5 mM). The filters were incubated on a shaker to achieve constant stirring. At desired time points the samples were taken from the basolateral chamber and [^{14}C]mannitol was measured in a β-liquid scintillation counter.

Activation of *Cl^- efflux* pathways in response to mastoparan was measured as previously described by Venglarik *et al*. using ^{125}I as tracer [19]. Efflux rate constants were expressed as percent per hour.

2.5. Measurement of cAMP

T84 monolayers were stimulated with mastoparan (10 μM) for 5 min. The cells were rinsed with ice-cold PBS, scraped from culture dishes and briefly sonicated at 4°. cAMP levels in the extracts were determined using a commercially available enzyme-linked immunoabsorbant assay kit. Samples and standards were prepared according to instructions for nonacetylation assays.

2.6. Measurement of intracellular calcium

The levels of intracellular free calcium were measured by the Fura-2 method. The cells were trypsinized with 0.25% trypsin, 0.1% EDTA, washed three times with Dulbecco's PBS and loaded with 10 μM Fura-2 AM in PBS containing 1 mM Ca^{2+} and Mg^{2+}, for 45 min at 37°. To remove free Fura-2, the cells were washed three times with PBS. Calcium was measured in PBS in a Hitachi fluorescence spectrophotometer model f-2000. Excitation wavelength was 340 and 390 nm, emission wavelength was 510. The optimal excitation of the sample was estimated by excitation wavelength scan from 300 to 400 nm.

2.7. Determination of inositol phosphates

To study the generation of inositol phosphates, confluent T84 monolayers grown on filters (Millipore, 45 μm, 35 mm diameter) were preincubated for 72 hr with inositol-free DMEM/F-12 mix, supplemented with 5% dialyzed NCS containing 20 μCi mL^{-1} myo-[^{2}H]inositol. Before stimulation, the medium containing radiochemicals was removed and the cells washed three times with Ringer solution containing 10 mM glucose. The cells were stimulated in Ringer solution for 15 min at 37°. This was terminated by aspiration of the buffer and addition 0.5 mL of ice-cold phytic acid (150 mM) containing 10% trichloroacetic acid. After 45 min incubation at 4° the cells were scraped from the filter transferred into Eppendorf cups, briefly sonicated, then 1 mL ice-cold Freon/Tri-*n*-octylamine (3:1) was added. The samples were mixed and the solution was allowed to settle until two phases were separated. The upper phase was transferred into centrifugal filtration cups (Ultrafree-MC, 45 μm, Millipore) and centrifuged at 500 *g* for 5 min. The inositol phosphates from the filtrates were resolved by HPLC on a 4.6 mm × 250 mm Absorbosphere SAX column (Alltech). Eluation was performed with a linear gradient to 0.5 M ammonium dihydrogenphosphate (pH 3.8) over 100 min with a flow of 1 mL min^{-1}. To detect radioisotopes, scintillation cocktail (Optiflow-safe, EG&G Berthold, Bad Wildbad) was added at a rate of 3 mL min^{-1}. Radioactivity in the effluent was measured by a radioisotope detector equipped with a 1 mL flow-through cell (EG&G Berthold, Bad Wildbad). Inositol phosphates were identified by comparison with elution times of radiolabeled standards.

2.8. F-actin/G-actin measurement

The F-actin and the G-actin content of the cells were measured indirectly by the method of Goldblum *et al*. F-actin was determined by its ability to bind rhodamine-labeled phalloidin [20]. For both F-actin and G-actin measurements, cells were grown on filters (0.45 μm, Millipore) and were stimulated in bicarbonate buffered Ringer solution, supplemented with 10 mM glucose. To determine F-actin, samples were taken 5, 15, 30, 45 and 60 min after stimulation. The stimulation was stopped by rinsing filters with ice-cold PBS and subsequent incubation with 3.7% formaldehyde solution in PBS for 15 min. The cells were permeabilized with imidazole buffer (75 mM KCl, 3 mM $MgSO_4$, 0.2 mM EGTA, 0.2 mM DTT, 10 mM imidazole, 0.1 mM PMSF, 10 μg mL^{-1} aprotinin) for 10 min, three times washed with PBS and incubated protected from light with 5 U mL^{-1} rhodamine phalloidin in PBS for 30 min. After washing three times with PBS the bound rhodamine was extracted overnight with 1 mL ethanol per filter. After centrifugation at 10,000 *g* for 1 min the rhodamine content of the supernatant was measured at 563 nm with an excitation wavelength of 542 nm with a fluorescence spectrophotometer (Hitachi f-2000).

G-actin was determined indirectly by its ability to inhibit DNAse. Cells were stimulated for 45 min and filters were then rinsed twice with ice-cold PBS. Cells were permeabilized with lysis buffer (2 mM $MgCl_2$, 2 mM EGTA, 0.5 mM DTT, 0.2 mM ATP, 0.1 mM PMSF, 1% (v/v) Triton X-100 in PBS) for 1 min. The solution was centrifuged for 5 min at 4000 *g* and 10 μL of the supernatant used for the DNAse assay. One millilitre DNA solution (0.2 mM Tris–HCl pH 7.5, 5 mM $MgSO_4$, 1.8 mM $CaCl_2$, 80 μg mL^{-1} calf thymus DNA, stirred at 4° for 48 hr) was pipetted into a quartz cuvette and 10 μL of the samples or the G-actin standard added. To start the assay 10 μL of DNAse-solution (125 mM Tris–HCl pH 7.5, 5 mM $MgCl_2$, 2 mM $CaCl_2$, 1 mM NaN_3, 0.1 mM PMSF, 10 mg mL^{-1} DNAse I, type IV; diluted 1:100 with 30 mM NaCl, 20 mM imidazole pH 7.5, 15% (v/v) glycerol) were added and the increase in extinction was measured for 1 min at 260 nm. For G-actin standard bovine muscle actin was used in

concentrations of 5–200 μg mL^{-1}. The G-actin content of the samples was determined by comparing the change in extinction (ΔE min^{-1}) of samples with the actin standards.

2.9. ADP-ribosylation assay and SDS/polyacrylamide gel electrophoresis

The ADP-ribosylation was carried out as described by Aktories [21]. Hundred micrograms of protein in 50 μL H_2O was transferred to an Eppendorf vial; 45 μL ribosylation buffer containing 100 mM Tris–HCl pH 7.5, 10 mL EDTA, 4 mM $MgCl_2$, 2 mM DTT, 20 mM thymidine, 2 mM ATP, 0.2 mM GTP, 0,02% (w/v) SDS, 2 mM PMSF, 20 μg mL^{-1} leupeptin, 2% (v/v) aprotinin, and 20 μCi mL^{-1} [^{32}P] NAD were added. The reaction was started by the addition of 5 μL exoenzyme C_3 (100 μg mL^{-1} in PBS) and the solution incubated at 37° for 45 min. The reaction was terminated by adding 200 μL of ice-cold trichloracetic acid. The precipitated protein was gained by centrifugation (5000 *g*). The pellet was dissolved in 25 μL Tris-Solution (1 M) and 25 μL of the electrophoresis buffer was added. SDS/polyacrylamide gel electrophoresis was performed according to Laemmli [22]. Gels were stained with Coomassie blue, destained and subjected to autoradiography for 12–48 hr.

2.10. Statistical analysis

Data given were means of at least three independent experiments ± standard error of the mean. Statistical significance was calculated using the *t*-test for unpaired values. $P < 0.05$ was considered significant.

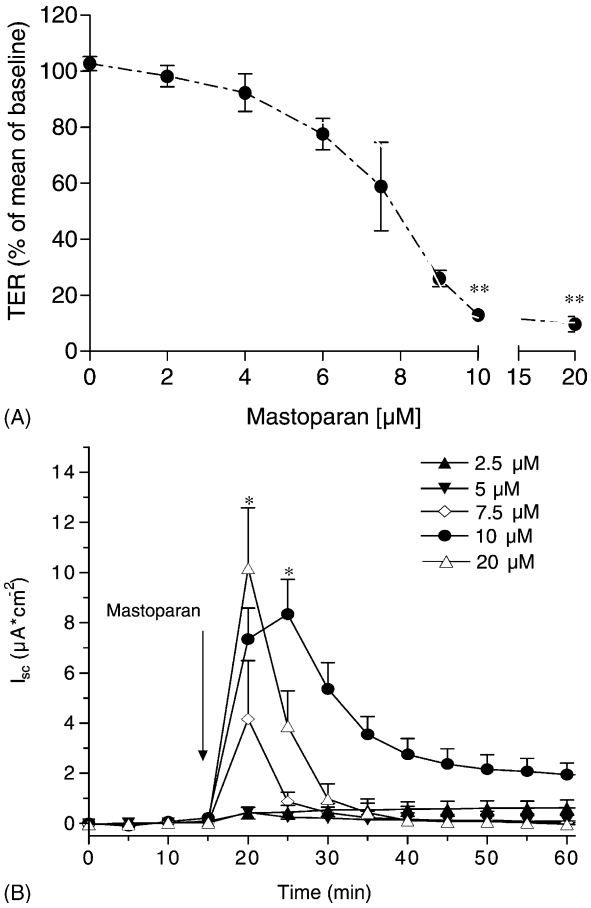

Fig. 1. (A) Effect of mastoparan on the transepithelial resistance (TER) of T84 monolayers. Concentrations <5 μM had no effect on TER. The IC_{50} was 7.8 μM (N = 4–7, $^{**}P < 0.01$ vs. control). (B) Mastoparan in concentrations higher than 5 μM induces a significant and transient increase in short circuit current (I_{sc}) (N = 3–12, $^{*}P < 0.05$).

3. Results

3.1. Effects and specificity of mastoparan

Mastoparan (mas) affected TER of T84 monolayers in a range from 5 to 10 μM. TER did not change when mastoparan was applied in concentrations less than 5 μM, whereas 10 μM mastoparan decreased the resistance to approximately 20% of initial values (Fig. 1A). TER values did not change when mastoparan was added in concentrations lower than 5 μM. The half-maximum response was obtained at a concentration of 7.8 μM and maximal effect was achieved at 15 μM (Fig. 1A). The mastoparan-induced SCC also increased in the same, dose-dependent, manner (Fig. 1B). TER as well as short circuit remained unaffected, when mastoparan was applied from the basolateral side (data not shown). To exclude any unspecific effect of mastoparan on TER, we compared effects of mastoparan and its inactive analogon mas17. Unlike mastoparan, mas17 did not affect TER or SCC indicating that the positive charge of this molecule did not influence the integrity of the monolayer (data not shown).

Cytotoxity of mastoparan was assessed by ethidium homodimer uptake (data not shown) and by the preservation of carbachol- or forskolin-stimulated SCC at the end of each experiment. We also verified the lack of leakage of lactate dehydrogenase, a marker for damaged membranes, from the cytosol in mastoparan-stimulated cells (data not shown).

Under control conditions the transepithelial conductance was $G_t = 0.51$ mS cm^{-2}. Paracellular conductance, calculated from the linear regression of the G_t vs. I_{sc} after addition of nystatin, amounted to $G_p = 0.495$ mS cm^{-2} (Fig. 2). Thus, transcellular conductance, calculated as difference between G_t and G_p, was $G_c = 0.015$ mS cm^{-2}. Ninety minutes after stimulation with mastoparan, when the SCC had already returned to baseline levels, the stimulated cells revealed a paracellular conductance of $G_p = 2.08$ mS cm^{-2}, whereas the transcellular conductance again amounted to $G_c = 0.013$ mS cm^{-2}. In accordance with the calculated increase in paracellular conductance, measurements of the paracellular flux with [^{14}C]mannitol showed increased permeability after stimulation with mastoparan (Fig. 3) as well. These data, expressed as a percentage of donor reservoir, showed a

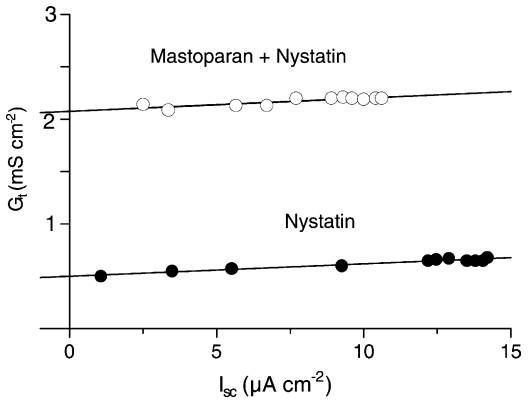

Fig. 2. Transepithelial resistance in T84 cells. Nystatin-induced (400 U mL^{-1} nystatin) changes of I_{sc} and G_t show linear relationship. The closed circles (●) represent control experiments and the open circles (○) experiments with continued mastoparan stimulation. From the transepithelial conductance vs. I_{sc} plot, paracellular conductance was calculated to values of $G_s = 0.495$ mS cm^{-1} before addition of mastoparan and $G_s = 2.08$ mS cm^{-2} (480 Ω cm^2) after stimulation (N = 3).

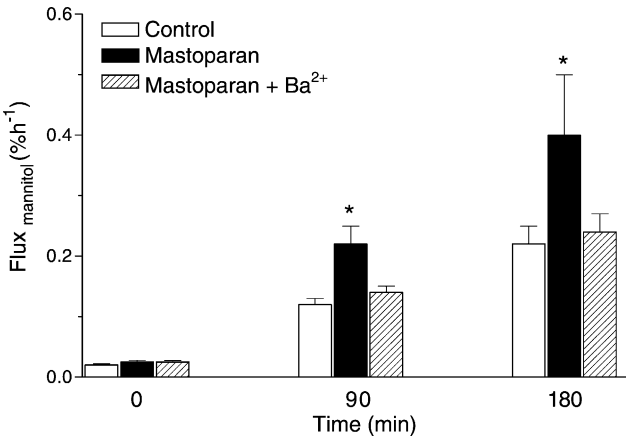

Fig. 3. Paracellular permeability measured by flux of [^{14}C]mannitol (N = 4–5, $^*P < 0.05$).

2-fold increase in permeability (control: 0.204 ± 0.023%, mastoparan: 0.410 ± 0.113%). The [^{14}C]mannitol flux rates increased slowly, reaching a maximum level after 180 min. Preincubation with 2 mM Ba^{2+} reduced the mastoparan-induced mannitol flux to control levels (0.193 ± 0.017%).

3.2. Effect of mastoparan on chloride secretion

To determine which ions are involved in the mastoparan-induced increase in SCC, the possible involvement of Cl^- secretion was investigated. Cl^- was expected to be taken up from the basolateral solution *via* a $Na^+/K^+/2Cl^-$ co-transporter and to be secreted to the luminal bath *via* apical Cl^- channels. Accordingly, a reduction in Cl^- current was expected either after blocking the $Na^+/K^+/2Cl^-$ co-transporter with bumetanide, after removal of Cl^- from the serosal bath, or blocking apical Cl^- channels with specific inhibitors. Blocking of the $Na^+/K^+/2Cl^+$ co-transporter with 100 μM bumetanide 10 min before stimulation reduced the mastoparan-induced chloride secretion from 8.34 ± 1.38 to 6.40 ± 0.69 μA cm^{-2} ($P < 0.05$). Similarly, substitution of Cl^- by isethionate in the basolateral solution reduced the mas-stimulated peak value of SCC from 8.34 ± 1.38 to 3.34 ± 1.02 μA cm^{-2} ($P < 0.01$) (Table 1). As a verification, bumetanide or basolateral Cl^--free buffer also reduced the forskolin-induced Cl^- current from 18.05 ± 1.5 to 9.90 ± 1.0 μA cm^{-2} ($P < 0.01$) and from 18.05 ± 1.5 to 1.53 ± 0.273 μA cm^{-2} ($P < 0.01$), respectively (data not shown). Like bumetanide, basolateral Cl^--free buffer did not affect changes in TER induced by mastoparan or forskolin significantly (data not shown). Additional experiments with *N*-phenylanthranilic acid, a specific inhibitor of bumetanide-insensitive Cl^- transport, showed no changes of the mastoparan or forskolin-induced SCC (Table 1).

In agreement with the above data, mastoparan increased iodide secretion of the cells preincubated with ^{125}iodide (data not shown), indicating that stimulation of chloride secretion contributes to the increase in SCC. Prior to stimulation, the secretion was 0.128 ± 0.069 pCi min^{-1} cm^{-2} and increased 2.9-fold to 0.376 ± 0.048 pCi min^{-1} cm^{-2}. Nevertheless, inhibition of chloride secretion had no effect on the changes in TER after stimulation with mastoparan. In contrast to successful reduction of SCC by reducing basolateral Cl^- entry, blocking of the apical Cl^- channels by known Cl^- channel blockers NPPB (100 μM), DIDS (100 μM), and glibenclamide (100 μM) did neither reduce chloride secretion significantly nor was the mastoparan-induced change in TER affected (data not shown). Thus, NPPB, DIDS or glibenclamide sensitive Cl^-channels seem not to be involved in the SCC induced by mastoparan.

3.3. Inhibition of potassium efflux

To test whether the SCC remaining after inhibition of basolateral Cl^- uptake was partly generated by basolateral K^+ efflux, the cells were incubated with the potassium

Table 1
Bumetanide, as well as basolateral Cl-free medium decreased significantly the mastoparan-induced I_{sc} whereas *N*-phenylanthranilic acid had no inhibitory effect on the mastoparan-induced I_{sc} (N = 3–8; $P < 0.05$).

	mas + Cl^- bl	mas + Cl^--free solution bl	mas + *N*-Phenylan-thranilic acid	mas + bumetanide
$I_{sc_{max}}$ (μA cm^{-2})	8.34 ± 1.38	3.34 ± 1.02**	8.3 ± 1.9	6.40 ± 0.69*

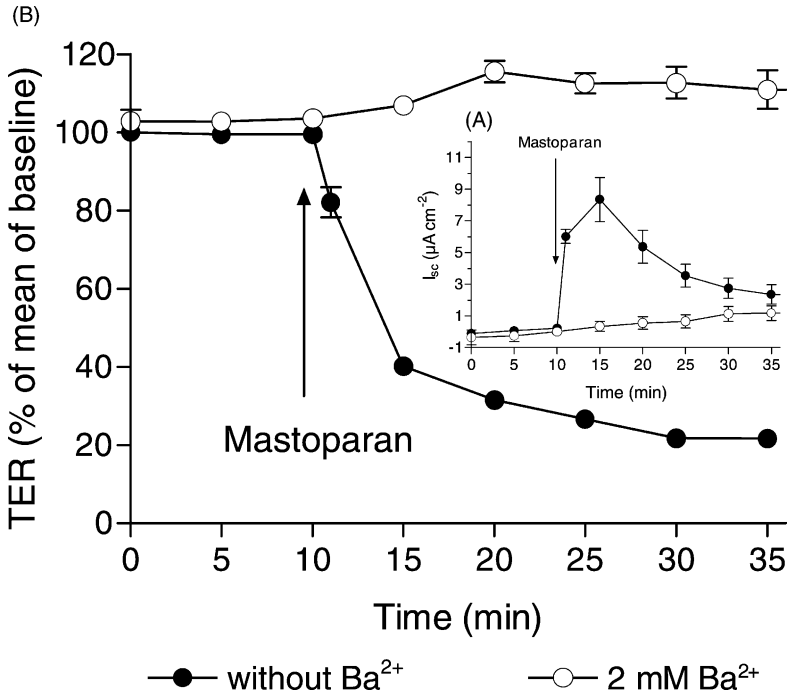

Fig. 4. Effects of mastoparan are modulated by changes in K^+ conductance of the plasma membrane. Ba^{2+} (2 mM), a blocking agent for all K^+ channels, abolished the mastoparan-induced short circuit current (A) as well as changes in TER (B).

channel blocker Ba^{2+} prior to stimulation with mastoparan. The Ca^{2+} concentration in the basolateral bath remained hereby unchanged. Preincubation with 2 mM Ba^{2+} completely abolished the mastoparan-induced changes in SCC. This indicates that basolateral efflux of K^+ ions is responsible for the mastoparan-induced changes in SCC (Fig. 4A), most likely caused by an increased driving force for apical chloride exit. Correspondingly, elevation of K^+ concentration in the basolateral reservoir from 2.4 to 10 mM reduced the mastoparan-induced SCC from 7.77 ± 1.18 to 2.12 ± 0.47 µA cm^{-2}, whereas 110 mM K^+ totally abolished the increase in SCC (0.177 ± 0.09 µA cm^{-2}) (Table 2). While reduction of the basolateral Cl^- uptake did not influence the TER response, basolateral application of Ba^{2+} abolished the mastoparan-induced changes of TER (Fig. 4B). Similarly, elevation of electrochemical K^+ concentration reduced the mastoparan-induced decrease of TER. In the presence of 2.4 mM K^+, TER decreased to 20% of control, in the presence of 10 mM K^+ to 59% while in the presence of 110 mM K^+ no decrease was observed (110%) (Table 2).

Table 2
Increasing concentrations of basolateral K^+ reduced the mastoparan-induced I_{sc} and the decrease in TER (N = 4–6)

	mas + 2.4 mM K^+ bl	mas + 10 mM K^+ bl	mas + 110 mM K^+ bl
TER (% mean of baseline)	20	59	110
$I_{sc_{max}}$ (µA cm^{-2})	7.77 ± 1.18	2.12 ± 0.47**	0.18 ± 0.09***

3.4. Effect of mastoparan on intracellular second messengers

To elucidate the intracellular signal transduction pathways mediating the effect of mastoparan, we measured intracelluar cAMP, cGMP and intracellular free Ca^{2+} levels as well as inositol phosphates after the cells were treated with mastoparan. Fig. 5 shows the intracellular cAMP and cGMP levels under control conditions and after stimulation with mastoparan: 10 mM mastoparan had neither any effect on the cAMP level (5.85 ± 0.121 pmol mg^{-1} protein) nor on the intracellular cGMP level. Vasoactive intestinal peptide (10^{-7} µM) increased intracellular cAMP approximately 20-fold after 5 min.

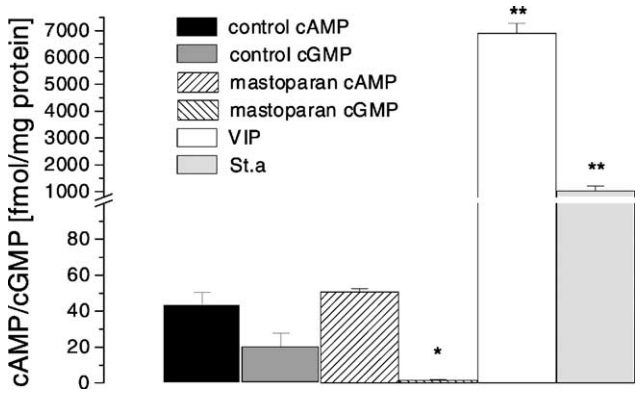

Fig. 5. Effect of mastoparan, vasointestinal peptide (VIP) and St.a on intracellular second messenger concentrations (cAMP and cGMP) in T84 cells. Values are given as pmol cAMP or cGMP per milligram protein. Mean ± SEM, N = 4. $^{**}P < 0.01$; $^{*}P < 0.05$, both vs. control.

Mastoparan had no effect on the VIP-induced increase of cAMP (data not shown). Stimulation with *Staphylococcus aureus* toxin (St.a), a cGMP-dependent agonist, led to a significant increase of intracellular cGMP (1036 ± 177 fmol mg^{-1} protein, $P < 0.01$ vs. control). Stimulation with mastoparan however even caused a decrease in intracelluar cGMP (1.8 ± 0.1 fmol mg^{-1} protein, $P < 0.05$ vs. control).

The changes in free $[Ca^{2+}]_i$ measured with Fura-2 AM, are shown in Fig. 6. Addition of mastoparan resulted in a rapid increase in fluorescence from 13.21 to 16.92 (Fig. 6A), which did not decline during the observation period of 2 min, indicating that mastoparan induced a high and sustained increase in $[Ca^{2+}]_i$ from 214 nM to 728 μM. The cells stimulated with mastoparan showed only a minor additional increase in fluorescence when Triton X-100 was added in order to permeabilize cell membranes, and show maximum fluorescence ($E_{max} = 1.2$ mM). The inactive mastoparan analogon mas17, a tetradecapeptide differing from mastoparan only in two amino acids, did not alter basal fluorescence except for a small initial decrease in fluorescence probably due to quenching (Fig. 6B). Preincubation in 2 mM Ba^{2+} as well as extracellular 50 mM K^+ prevented an increase in fluorescence when the cells were subsequently stimulated with mastoparan (Fig. 6C). To distinguish between Ca^{2+} release from intracellular stores and influx of extracellular Ca^{2+} into the cells, the cells were stimulated with mastoparan in Ca^{2+}-free medium. As illustrated in Fig. 6D, mastoparan caused a decrease rather than an increase in fluorescence in Ca^{2+}-free buffer, showing that the increase in $[Ca^{2+}]_i$ resulted mainly from influx of extracellular Ca^{2+}. Addition of 2.4 mM Ca^{2+} to the Ca^{2+}-free buffer resulted in an immediate increase in fluorescence in mastoparan-prestimulated cells, corresponding to a rise from 226 nM to 605 μM.

Although mastoparan increased intracellular Ca^{2+}, experiments in basolateral Ca^{2+}-free medium showed no significant alteration of the mastoparan-induced effect on TER ($31.5 \pm 5.2\%$ vs. $35 \pm 9\%$ of mean of baseline after 10 min stimulation). Preincubation of cells with 100 μM BAPTA to complex intracellular free Ca^{2+} did also not alter the mastoparan-induced change in TER (Fig. 7).

Stimulation with mastoparan did not alter the generation of inositol phosphates. In comparison to controls, there was no detectable increase of inositol-1,4,5-trisphosphate or inositol-1,3,4-trisphosphate 1 min or 30 min after stimulation (data not shown). Rapid metabolization of inositol phosphates could be excluded, since there was also no increase in other inositol phosphates such as $InsP_2$, $InsP_4$ or $InsP_6$. Carbachol-stimulated cells, used as positive control, showed increased inositol-1,4,5-trisphosphate and

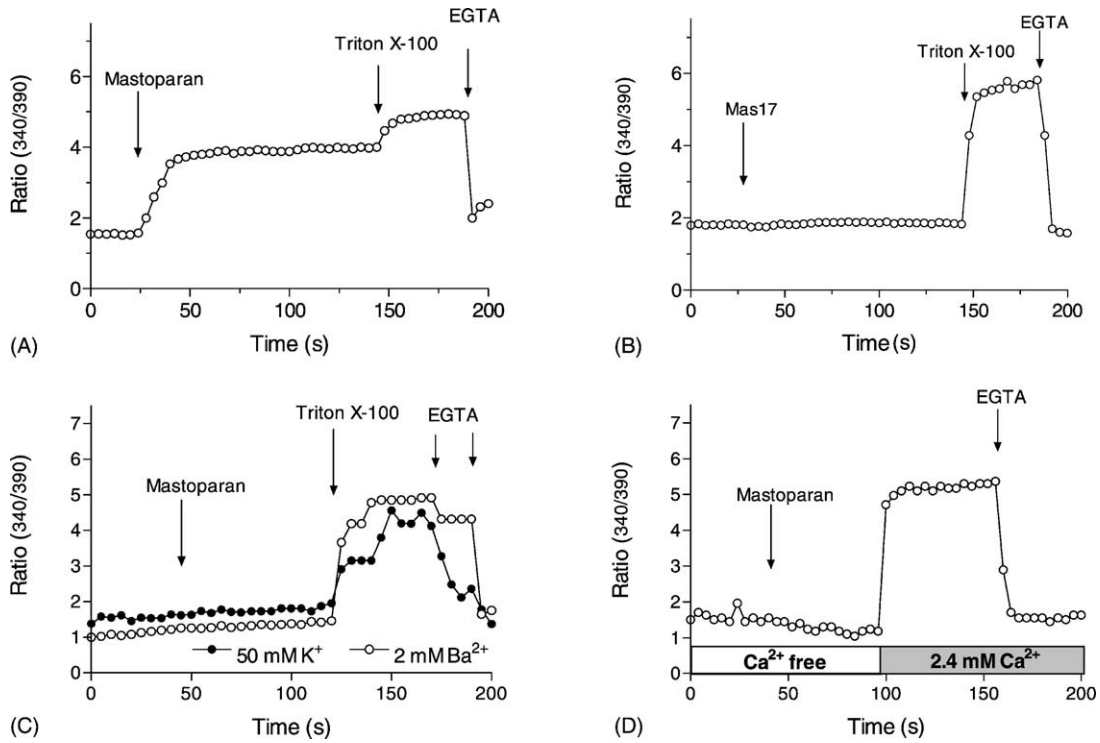

Fig. 6. Effect of mastoparan on free cytosolic Ca^{2+} concentrations ($[Ca^{2+}]_i$) in T84 cells. $[Ca^{2+}]_i$ was monitored as ratio of fluorescence at excitation wavelengths of 380 and 340 nm (I_{380}/I_{340}). Mastoparan and mas17 were added at the time indicated by the left arrows. Triton X-100 (0.1%) and EGTA (2 mM) were added at the end of each experiment as positive and negative controls, respectively. (A) Apical addition of mastoparan (15 μM), (B) addition of the mastoparan analogue mas17 (15 μM). (C) Both basolateral addition of Ba^{2+} (2 mM) and decrease in basolateral K^+ concentration (50 mM) prevented the mas-induced influx of Ca^{2+}. (D) In the presence of extracellular EGTA (2 mM) mastoparan failed to increase ($[Ca^{2+}]_i$). Each graph represents N = 3 experiments.

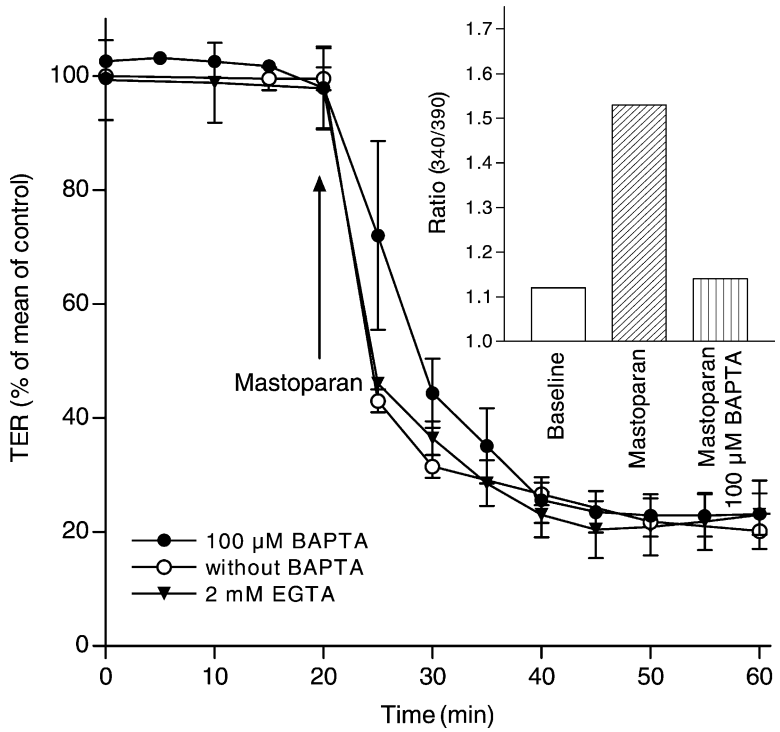

Fig. 7. Preincubation with 1,2-bis(2-aminophenoxy)ethane-*N*,*N*,*N*′,*N*-tetraacetic acid (BAPTA) does not alter the ability of mastoparan to decrease resistance of T84 cell monolayers. Cells were preincubated for 45 min with 0.5 mM BAPTA before the cells were mounted in Using chambers. Values are expressed as resistance relative to base baseline and as means ± SD for at least five experiments. Insert: effect of BAPTA on mastoparan increased free cytosolic Ca^{2+} concentrations ($[Ca^{2+}]_i$) in T84 cells. $[Ca^{2+}]_i$ was monitored as ratio of fluorescence at excitation wavelengths of 380 and 340 nm (I_{380}/I_{340}).

inositol-1,4,5,6-tetrakisphosphate levels and inositol-1,3,4-trisphosphate, as a metabolite of Ins(1,4,5)P_3 and InsP_4 turnover as well.

3.5. Effect of mastoparan on F- and G-actin and influence of the actin cytoskeleton

Stimulation with mastoparan led to biphasic changes in the amount of actin filaments. Within the first 20 min there was an increase in F-actin to 122% as compared to controls (Fig. 8A). The temporary increase in F-actin content was followed by a rapid decrease: 30 min after stimulation, F-actin content was reduced to 75%, declining further to 64% after 60 min. Control cells showed a decrease in F-actin of only 4% during 60 min incubation.

The F-actin pool was measured 45 min after stimulation when TER was at a minimum. In contrast to F-actin, there was an increase in G-actin content to 117.4 ± 11% compared to controls (99.9 ± 6.8%) (Fig. 8B). Ba^{2+} inhibited the mastoparan-induced increase in G-actin (95.6 ± 6%) and the K^+ ionophore valinomycin as a positive control also increased G-actin to 121.7 ± 7.9%.

3.6. Interaction of mastoparan with GTP-binding proteins

As the small GTPase Rho is known to be an important regulator of tight junctions, the influence of mastoparan on Rho proteins was estimated by determination of the Rho/Rho-GDI complex. Therefore, Rho-GDI was immunoprecipitated and the precipitates were [^{32}P]ADP-ribosylated and visualized by autoradiography. After stimulation with mastoparan (10 µM) significantly more Rho-GDI complexes could be detected (174% ± vs. control $P < 0.01$) in T84 cells (Fig. 9).

4. Discussion

We provided several lines of evidence showing, first, that mastoparan decreases the TER and increases the paracellular conductance in T84 cell monolayers, the effect being independent of the presence of chloride in the extracellular medium, but completely abolished by blockade of basolateral K^+-channels. Second, that mastoparan acts primarily *via* activating K^+ channels with a secondary Cl^- secretion and Ca^{2+} influx. And third, that this drug inactivates RhoA and thereby causes a biphasic rearrangement of actin filaments and increased globular actin content in T84 cells. This study therefore elucidates the mechanisms by which mastoparan may enhance intestinal absorption of various drugs in humans, and is of importance both in physiology and in pharmacology.

T84 cells have been widely used as a model system to define regulatory mechanisms for both Cl^- secretion and barrier function [23–25]. By using these cells grown as

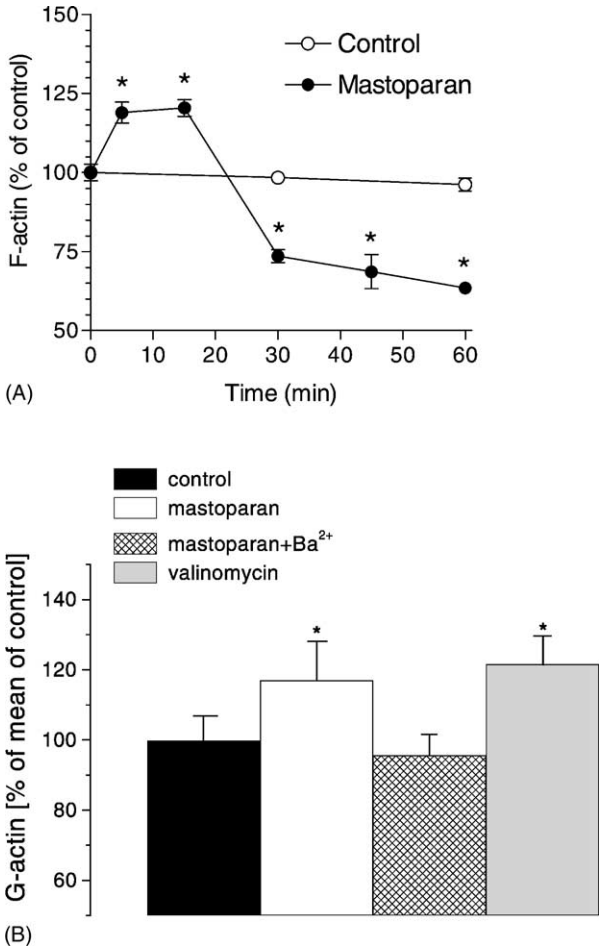

Fig. 8. (A) Disassembling of filamentous actin after stimulation with mastoparan. (B) The content of G-actin in the cells 45 min after stimulation (N = 5, $^{*}P < 0.05$).

monolayers, we were able to show that their stimulation with mastoparan decreases TER and increases the SCC, the decrease in TER being due to changes in paracellular conductance. Even if this technique has its limitations (as described by Kottra and Frömter [26]), the observed change in TER could not be due to a transcellular shunt for Cl^- or K^+, since the SCC already returned to baseline after nystatin treatment of the stimulated cells. Different polycations, like poly-L-lysine, alter transepithelial permeability unspecifically, likely by electrostatic binding to membrane proteins constituting the tight junctions. As a result, their functional properties are altered [24–27]. Since mastoparan has several positive charges, we investigated the possibility that it may affect transepithelial permeability by some comparable mechanism. Stimulation of the cells with its inactive analogue, mas17, with one additional positive charge compared to mastoparan, did not affect TER. These data imply that no essential change in membrane integrity or other unspecific effect could be caused by mastoparan and its charged analogues. The mastoparan-induced decrease in TER was missing when the drug was applied from the basolateral side, indicating that there was no leakage of ions or molecules from the cells, as it was supposed earlier [28]. In accord to this, no leakage of lactate dehydrogenase from the cytosol, as a marker of membrane damage, could be detected in mastoparan-treated cells.

Further experiments were aimed to clarify the modes of action responsible for the mastoparan-induced increase in SCC and the decrease in TER. In the first series of experiments we observed that (i) blockade of basolateral Cl^- uptake inhibited a large part of SCC, but did not influence TER reduction; (ii) blockade of basolateral K^+ channels by Ba^{2+} fully prevented both the increase in SCC and the decrease in TER; (iii) the rise of $[Ca^{2+}]$ after mastoparan was completely inhibited by Ba^{2+}. And finally (iv) treatment with mastoparan induced an almost 2-fold increase of GDI-complexed Rho.

Since the Cl^- secretion is not a prerequisite for the decrease in TER, the increased paracellular permeability did not result from cell shrinkage, as postulated by Winter *et al*. [10]. The primary effect of mastoparan is an increase

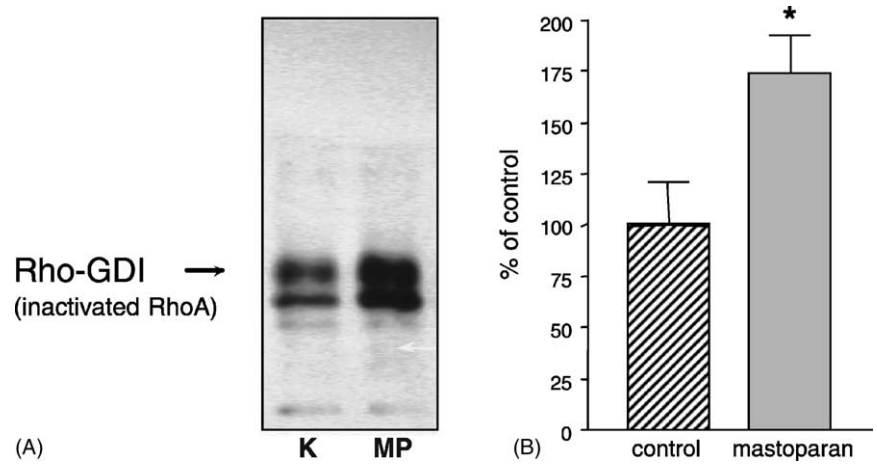

Fig. 9. Determination of the Rho/Rho-GDI complexes after stimulation with mastoparan. (A) Rho-GDI was immunoprecipitated and the precipitates were [^{32}P]ADP-ribosylated and visualized by autoradiography after electrophoresis. (B) After stimulation with mastoparan (10 μM) (174 ± 19% vs. control $P < 0.01$).

in K^+ conductance, which is inhibited by both K^+ channel blocker Ba^{2+} and by increasing concentrations of extracellular K^+. This also shows that mastoparan does not directly activate Cl^- channels. However, it remains unknown whether Cl^- channels were activated indirectly (due to increased intracellular Ca^{2+}), or whether the increased Cl^- carried SCC after mastoparan results from an increased driving force for apical anion secretion due to basolateral membrane hyperpolarization after opening K^+ channels.

The activation of basolateral K^+ channels also induced an increased paracellular permeability which could be fully prevented by Ba^{2+}. Thus, activation of these K^+ channels is likely to be the primary signal for the decrease in TER, and may result in the activation of further signal transduction mechanisms. One subsequent effect of activated K^+ channels was the activation of Ca^{2+} channels, which led to an influx of extracellular Ca^{2+}. Both blocking of K^+ channels with Ba^{2+} as well as increased extracellular K^+ concentration inhibited the rise in $[Ca^{2+}]_i$. However, it seems unlikely that voltage-dependent Ca^{2+} channels as described by Leipziger *et al*. in HT29 cells regulate the mastoparan-induced Ca^{2+} influx, since preincubation of cells with BAPTA-AM could not inhibit the mastoparan-induced change in TER [29]. It has to be considered that basolateral Ca^{2+} channels may select Ba^{2+} over Ca^{2+} in experiments where Ba^{2+} was used to block basolateral K^+ channels and subsequently block the influx of Ca^{2+}. However, addition of EGTA to the basolateral side could reverse the mastoparan-induced influx of calcium, therefore providing a strong evidence that Ba^{2+} acts as K^+ channel blocker rather than being a substitute for Ca^{2+} ions.

In spite of extensive research over the past decades, the exact modes of action of mastoparan have not yet been fully elucidated. The question that may arise is whether its effects described in this study are indeed specific and if they are due to distinct mastoparan-induced signal transduction pathways in the cell. Our data indeed favour this hypothesis, since mastoparan-induced change in paracellular conductance required no rise in intracellular free Ca^{2+} or inositol phosphates and was not cAMP- and cGMP-dependent (Figs. 5–6).

It appeared therefore likely that reorganisation of the cytoskeleton due to mastoparan may be involved, at least in part, in the effects of this drug we described. Similar was described in human neutrophils [30] and also suggested by Madara and co-workers [16,17] and Ries *et al*. [25]. Our data showed that a possible regulator of the mastoparan-induced effects on the cytoskeleton is the small GTP-binding protein RhoA, which regulates the organization of the actin filaments [31–34]. In confluent cell layers opening of the tight junctions, e.g. by bacterial toxins resulting in decreased barrier function can be explained by inactivation of Rho proteins [35,36]. Associations of RhoA with actin-binding proteins, e.g. members of the ERM (ezrin-radixin-moesin) family in endothelial monolayers is known [37] as well as Rho driven interaction between ERM proteins and the plasma membrane [38]. A Rho kinase (ROCK) as a downstream effector of Rho regulates tight junction function and is necessary for tight junction assembly in T84 cells [39]. We showed that RhoA is concentrated at the tight junction and adhesion plaques of intestinal tight junctions and that it is co-localized with ZO-1, a zonula occludens protein and E-cadherin, a zonula adhaerens protein (unpublished data). Mastoparan has been demonstrated to interact with small GTP-binding proteins Rho and Rac in several cell types [15]. Although mastoparan is a known activator of trimeric G-proteins [5,40–43] in several cell types, Rho together with a trimeric G-protein regulates changes in the actin cytoskeleton observed in activated mast cells [44,45]. In chromaffin cells, the mastoparan-induced inhibition of secretion can be partially reversed by agents known to affect the assembly of actin and by the *Clostridium botulinum* C3 ADP-ribosyltransferase, which specifically inactivates the small GTPase Rho by ADP-ribosylation [46,47]. In agreement to these studies, our experiments showed that mastoparan induced a significant rise in Rho-GDI complexes in T84 cells, indicating the inactivation of Rho proteins, and this inactivation—perhaps also involving trimeric G-proteins—may trigger the above discussed cascade and result in an opening of tight junctions/an increase in paracellular permeability.

Acknowledgments

These studies were supported by the Else Kröner-Fresenius-Foundation (Bad Homburg, Germany).

References

[1] Sigthorsson G, Tibble J, Hayllar J, Menzies I, Macpherson A, Moots R, Scott D, Gumpel MJ, Bjarnason I. Intestinal permeability and inflammation in patients on NSAIDs. Gut 1998;43:506–11.
[2] Aridor M, Rajmilevich G, Beaven MA, Sagi-Eisenberg R. Activation of exocytosis by the heterotrimeric G-protein Gi3. Science 1993;262:1569–72.
[3] Danilenko M, Worland P, Carlson B, Sausville EA, Sharoni Y. Selective effects of mastoparan analogs: separation of G-protein-directed and membrane-perturbing activities. Biochem Biophys Res Commun 1993;196:1296–302.
[4] Emadi-Khiav B, Mousli M, Bronner C, Landry Y. Human and rat cutaneous mast cells: involvement of a G-protein in the response to peptidergic stimuli. Eur J Pharmacol 1995;272:97–102.
[5] Higashijima T, Burnier J, Ross EM. Regulation of Gi and Go by mastoparan, related amphiphilic peptides, and hydrophobic amines. Mechanism and structural determinants of activity. J Biol Chem 1990;265:14176–86.
[6] Klinker JF, Hageluken A, Grunbaum L, Heilmann I, Nurnberg B, Harhammer R, Offermanns S, Schwaner I, Ervens J, Wenzel-Seifert K. Mastoparan may activate GTP hydrolysis by Gi proteins in HL-60 membranes indirectly through interaction with nucleoside diphosphate kinase. Biochem J 1994;304(Pt 2):377–83.
[7] Naim M, Seifert R, Nurnberg B, Grunbaum L, Schultz G. Some taste substances are direct activators of G-proteins. Biochem J 1994;297(3):451–4.

[8] Ross EM, Higashijima T. Regulation of G-protein activation by mastoparans and other cationic peptides. Methods Enzymol 1994; 237:26–37.
[9] Gil J, Higgins T, Rozengurt E. Mastoparan, a novel mitogen for Swiss 3T3 cells, stimulates pertussis toxin-sensitive arachidonic acid release without inositol phosphate accumulation. J Cell Biol 1991;113: 943–50.
[10] Winter MC, Carson MR, Sheldon RA, Shasby DM. Mastoparan activates apical chloride and potassium conductances, decreases cell volume, and increases permeability of cultured epithelial cell monolayers. Am J Respir Cell Mol Biol 1992;6:583–93.
[11] Nakahata N, Ishimoto H, Mizuno K, Ohizumi Y, Nakanishi H. Dual effects of mastoparan on intracellular free Ca^{2+} concentrations in human astrocytoma cells. Br J Pharmacol 1994;112:299–303.
[12] Palant CE, Duffey ME, Mookerjee BK, Ho S, Bentzel CJ. Ca^{2+} regulation of tight-junction permeability and structure in Necturus gallbladder. Am J Physiol 1983;245:C203–12.
[13] Wheeler-Jones CP, Saermark T, Kakkar VV, Authi KS. Mastoparan promotes exocytosis and increases intracellular cyclic AMP in human platelets. Evidence for the existence of a Ge-like mechanism of secretion. Biochem J 1992;281(Pt 2):465–72.
[14] Hopkins AM, Li D, Mrsny RJ, Walsh SV, Nusrat A. Modulation of tight junction function by G-protein-coupled events. Adv Drug Deliv Rev 2000;41:329–40.
[15] Koch G, Haberman B, Mohr C, Just I, Aktories K. Interaction of mastoparan with the low molecular mass GTP-binding proteins rho/rac. FEBS Lett 1991;291:336–40.
[16] Madara JL, Moore R, Carlson S. Alteration of intestinal tight junction structure and permeability by cytoskeletal contraction. Am J Physiol 1987;253:C854–61.
[17] Madara JL. Intestinal absorptive cell tight junctions are linked to cytoskeleton. Am J Physiol 1987;253:C171–5.
[18] Amelsberg A, Schteingart CD, Stein J, Simmonds WJ, Sawada GA, Ho NF, Hofmann AF. Intestinal absorption of sodium dodecyl sulfate in the rodent: evidence for paracellular absorption. Am J Physiol 1997;272:G498–506.
[19] Venglarik CJ, Bridges RJ, Frizzel RA. A simple assay for agonist-regulated Cl and K conductance in salt secreting cells. Am J Physiol 1990;259(2 Pt 1):C358–64.
[20] Goldblum SE, Ding X Brann TW, Campbell-Washington J. Bacterial lipopolysaccharide induces actin reorganization, intercellular gap formation, and endothelial barrier dysfunction in pulmonary vascular endothelial cells: concurrent F-actin depolymerization and new actin synthesis. J Cell Physiol 1993;157(1):13–23.
[21] Aktories K. Clostridial ADP-ribosylating toxins: effects on ATP- and GTP-binding proteins. Mol Cell Biochem 1994;138:167–76.
[22] Laemmli UK. Cleavage of structural proteins during the assembly of the head of bacteriophage T4. Nature 1970;227:680–5.
[23] Matthews JB, Smith JA, Hrnjez BJ. Effects of F-actin stabilization or disassembly on epithelial Cl-secretion and Na-K-2Cl co-transport. Am J Physiol 1997;272:C254–62.
[24] Mandel KG, McRoberts JA, Beuerlein G, Foster ES, Dharmsathaphorn K. Ba^{2+} inhibition of VIP- and A23187-stimulated Cl-secretion by T84 cell monolayers. Am J Physiol 1986;250:C486–94.
[25] Ries J, Stein J, Traynor-Kaplan AE, Barrett KE. Dual role for AlF4(−)-sensitive G-proteins in the function of T84 epithelial cells: transport and barrier effects. Am J Physiol 1997;272:C794–803.
[26] Kottra G, Frömter E. Determination of paracellular shunt conductance in epithelia. Methods Enzymol 1990;191:4–27.
[27] Antonelli M, Olate J, Graf R, Allende CC, Allende JE. Differential stimulation of the GTPase activity of G-proteins by polylysine. Biochem Pharmacol 1992;44:547–51.
[28] Tanimura A, Matsumoto Y, Tojyo Y. Mastoparan increases membrane permeability in rat parotid cells independently of action on G-proteins. Biochem Biophys Res Commun 1991;177:802–8.
[29] Leipziger J, Fischer KG, Greger R. Voltage-dependent Ca^{2+} influx in the epithelial cell line HT29: simultaneous use of intracellular Ca^{2+} measurements and nystatin perforated patch-clamp technique. Pflugers Arch 1994;426:427–32.
[30] Norgauer J, Eberle M, Lemke HD, Aktories K. Activation of human neutrophils by mastoparan. Reorganization of the cytoskeleton, formation of phosphatidylinositol 3,4,5-trisphosphate, secretion up-regulation of complement receptor type 3 and superoxide anion production are stimulated by mastoparan. Biochem J 1992;282(Pt 2):393–7.
[31] Norman JC, Price LS, Ridley AJ, Hall A, Koffer A. Actin filament organization in activated mast cells is regulated by heterotrimeric and small GTP-binding proteins. J Cell Biol 1994;126:1005–15.
[32] Nusrat A, Giry M, Turner JR, Colgan SP, Parkos CA, Carnes D, Lemichez E, Boquet P, Madara JL. Rho protein regulates tight junctions and perijunctional actin organization in polarized epithelia. Proc Natl Acad Sci USA 1995;92:10629–33.
[33] Gopalakrishnan S, Raman N, Atkinson SJ, Marrs JA. Rho GTPase signaling regulates tight junction assembly and protects tight junctions during ATP depletion. Am J Physiol 1998;275:C798–809.
[34] Hopkins AM, Li D, Mrsny RJ, Walsh SV, Nusrat A. Modulation of tight junction function by G-protein-coupled events. Adv Drug Deliv Rev 2000;41:329–40.
[35] Lerm M, Schmidt G, Aktories K. Bacterial protein toxins targeting rho GTPases. FEMS Microbiol Lett 2000;188:1–6.
[36] Just I, Hofmann F, Genth H, Gerhard R. Bacterial protein toxins inhibiting low molecular mass GTP-binding proteins. Int J Med Microbiol 2001;291:243–50.
[37] Menager C, Vassy J, Doliger C, Legrand Y, Karniguian A. Subcellular localization of RhoA and ezrin at membrane ruffles of human endothelial cells: differential role of collagen and fibronectin. Exp Cell Res 1999;249:221–30.
[38] Kotani H, Takaishi K, Sasaki T, Takai Y. Rho regulates association of both the ERM family and vinculin with the plasma membrane in MDCK cells. Oncogene 1997;14:1705–13.
[39] Walsh SV, Hopkins AM, Chen J, Narumiya S, Parkos CA, Nusrat A. Rho kinase regulates tight junction function and is necessary for tight junction assembly in polarized intestinal epithelia. Gastroenterology 2001;121:566–79.
[40] Higashijima T, Uzu S, Nakajima T, Ross EM. Mastoparan, a peptide toxin from vasp venom mimics receptors by activating GTP-binding regulatory proteins (G-proteins). J Biol Chem 1988;263:6491–4.
[41] Bomsel M, Mostov K. Role of heterotrimeric G-proteins in membrane traffic. Mol Biol Cell 1992;3:1317–28.
[42] Mousli M, Bronner C, Bockaert J, Rouot B, Landry Y. Interaction of substance P, compound 48/80 and mastoparan with the alpha-subunit C-terminus of G-protein. Immunol Lett 1990;25:355–7.
[43] Ferry X, Brehin S, Kamel R, Landry Y. G-protein-dependent activation of mast cell by peptides and basic secretagogues. Peptides 2002;23:1507–15.
[44] Norman JC, Price LS, Ridley AJ, Hall A, Koffer A. Actin filament organization in activated mast cells is regulated by heterotrimeric and small GTP-binding proteins. J Cell Biol 1994;126:1005–15.
[45] Norman JC, Price LS, Ridley AJ, Koffer A. The small GTP-binding proteins, Rac and Rho, regulate cytoskeletal organization and exocytosis in mast cells by parallel pathways. Mol Biol Cell 1996;7:1429–42.
[46] Gasman S, Chasserot-Golaz S, Popoff MR, Aunis D, Bader MF. Trimeric G-proteins control exocytosis in chromaffin cells. Go regulates the peripheral actin network and catecholamine secretion by a mechanism involving the small GTP-binding protein Rho. J Biol Chem 1997;(277):20564–71.
[47] Gasman S, Chasserot-Golaz S, Hubert P, Aunis D, Bader MF. Identification of a potential effector pathway for the trimeric Go protein associated with secretory granules. Go stimulates a granule-bound phosphatidylinositol 4-kinase by activating RhoA in chromaffin cells. J Biol Chem 1998;273(27):16913–20.